

MSAGSM: Multi-Scale Attention Gated Shifting for Precise Event Spotting

Hao Xu

Deakin University
Melbourne, Australia

august.xu@research.deakin.edu.au

Mohamed Reda Bouadjenek

Deakin University
Melbourne, Australia

reda.bouadjenek@deakin.edu.au

Sam Wells

Paralympics Australia
Melbourne, Australia

sam.wells@paralympic.org.au

Richard Dazeley

Deakin University
Melbourne, Australia

richard.dazeley@deakin.edu.au

Sunil Aryal

Deakin University
Melbourne, Australia

sunil.aryal@deakin.edu.au

Abstract

Precise Event Spotting (PES) in sports videos requires frame-level recognition of fine-grained actions from single-camera footage. Existing PES models typically incorporate lightweight temporal modules such as the Gate Shift Module (GSM) or the Gate Shift Fuse to enrich 2D CNN feature extractors with temporal context. However, these modules are limited in both temporal receptive field and spatial adaptability. We propose a Multi-Scale Attention Gate Shift Module (MSAGSM) that enhances GSM with multi-scale temporal shifts and channel grouped spatial attention, enabling efficient modeling of both short and long-term dependencies while focusing on salient regions. MSAGSM is a lightweight, plug-and-play module that integrates seamlessly with diverse 2D backbones. To further advance the field, we introduce the Table Tennis Australia dataset, the first PES benchmark for table tennis containing over 4,800 precisely annotated events. Extensive experiments across four PES benchmarks demonstrate that MSAGSM consistently improves performance with minimal overhead, setting new state-of-the-art results. All code and datasets are publicly available at <https://anonymous.4open.science/r/MSAGSM-BOA4>.

1. Introduction

Detecting the precise moment when events occur in a video is a core challenge in video understanding, particularly in

the single camera setting commonly used in most sports recordings. Precise Event Spotting (PES) aims to localize and classify events at frame-level accuracy, typically within a 1–2 frame tolerance [12]. This fine-grained precision is critical in sports scenarios, where even a few frames of deviation can correspond to a different event entirely (see Figure 1). Accurate PES provides a strong foundation for downstream tasks such as ball tracking, player positioning, and automatic highlight generation. Moreover, precise spotting plays a vital role in post-game analysis by highlighting key moments and reducing the need to manually browse full-length videos. For instance, according to Table Tennis Australia’s sports analytics team, annotating events in a single match video can take 4–5 hours. Automating this process not only streamlines analysis but also enables timely feedback for athletes and coaches.

Recent advancements in video understanding have explored various approaches to this task, including transformer-based models [1, 54], multimodal methods [38, 43], and self-supervised frameworks [5]. Among these, E2E-Spot [12] has emerged as a strong baseline, inspiring several subsequent models such as the current state-of-the-art (SOTA) T-DEED [44], UGLF [37], and ASTRM [27]. A key component in E2E-Spot is the Gate Shift Module (GSM) [31], which enables 2D CNNs to learn temporal dynamics by shifting features across adjacent frames. While effective, GSM is limited in its temporal range and does not explicitly model longer-term dependencies.

Despite these advancements, PES remains a highly challenging task due to its unique characteristics. Events are

often difficult to distinguish from adjacent frames, sometimes even for human annotators without access to extended temporal context [44]. Moreover, different events may require varying amounts of temporal information to be correctly identified, further complicating model design. In addition to temporal reasoning, effective PES also demands accurate spatial attention: in sports videos, a large portion of each frame typically consists of background, making it essential for models to focus on small but informative regions such as the ball or a player’s hand position to make correct predictions. Another practical limitation lies in the availability of suitable datasets. Most publicly available sports video datasets are derived from broadcast footage of elite sports [9, 11, 12, 48], which are often professionally edited and filmed from ideal angles. However, in many real-world sports settings, such as local or developmental leagues, matches are recorded using handheld devices with varied perspectives, inconsistent quality, and frequent occlusions.

To address these challenges, we propose the Multi-Scale Attention Gate Shift Module (MSAGSM), a lightweight extension of GSM that overcomes its limitation of accessing only adjacent frames by incorporating multi-scale temporal shifts. To mitigate the noise introduced by larger temporal windows, we further design a channel-grouped spatial attention mechanism that learns spatial masks within channel groups to guide shifting, differing from transformer multi-head attention by avoiding costly query–key–value interactions. This design enables MSAGSM to capture longer-range dependencies while focusing on salient regions (e.g., ball or player positions), and it can be seamlessly integrated into 2D CNN backbones with minimal overhead compared to 3D models.

In addition, we introduce a new dataset for PES: the Table Tennis Australia (TTA) dataset, recorded and curated in collaboration with Paralympics Australia’s sports analysts, providing more realistic recordings compared to existing datasets. The dataset includes **39** games and a total of **4,878** annotated events across eight event types: serve, bounce, forehand, and backhand—each distinguished between the near and far sides of the table. To our knowledge, TTA is the first PES dataset specifically designed for table tennis. Compared to existing PES datasets, TTA is both sizable and challenging. Its scale is comparable to FineGym [28] and surpasses that of FigureSkating [11]. Moreover, unlike tennis [12], table tennis involves more densely packed, fine-grained events within shorter time spans, presenting a more demanding benchmark for PES.

Our main contributions are summarized as follows: (1) proposing **MSAGSM**, a lightweight module that combines multi-scale temporal shifts with spatial attention, and can be efficiently plugged into existing 2D CNN backbones; (2) introduce the **TTA** dataset, the first PES dataset for table

tennis, containing **39** games and **4,878** annotated events across eight classes; and (3) show that MSAGSM, when integrated with standard 2D backbones, achieves SOTA performance across multiple PES benchmarks, including TTA.

2. Related Work

Spatial-Temporal Modelling: Significant progress has been made in video understanding tasks, such as video classification and action recognition, driven by the development of deep CNNs and Transformer-based architectures [2, 6, 7, 20, 35]. One major challenge in these models is their high memory and computational requirements, which make them less suitable for deployment on resource-constrained devices compared to lightweight 2D CNNs.

To address this, recent research has focused on developing efficient and effective temporal modeling techniques built on top of 2D CNNs, minimizing computational complexity while retaining performance. Several approaches attempt to decompose 3D convolutions into separate spatial (2D) and temporal (1D) components [14, 24, 36, 45]. Others propose hybrid models that combine 3D CNNs with 2D CNNs to reduce overall cost [22].

A key advancement in this direction is the Temporal Shift Module (TSM) [17], which enables 2D CNNs to capture temporal information by shifting a portion of the feature channels along the temporal dimension. This parameter-free operation significantly improves efficiency over 3D or 2D+1D methods and demonstrated state-of-the-art performance in action recognition at the time. However, TSM’s shift mechanism is manually hardcoded and does not adapt to the input content.

To address this limitation, the GSM [31] was introduced. Built upon TSM, GSM employs an additional spatio-temporal 3D convolutional kernel as a gating mechanism to selectively decide which features to shift forward or backward based on contextual information. Its variant, Gate Shift Fuse (GSF) [32], adds a point-wise convolution block before and after the gating operation to enable interaction between spatial and spatio-temporal feature groups, further enhancing modeling capability.

Precise Event Spotting: In video understanding tasks such as video classification and action recognition, a common approach is to *sparsely* sample frames from the entire video [8, 15, 39]. In contrast, PES requires *dense* frame sampling, particularly for sports videos due to the fast motion and high frequency of events occurring within short time spans. Compared to Temporal Action Detection, which focuses on predicting temporal intervals of actions [18, 30], PES aims to identify actions using a single key frame. This is especially relevant in sports scenarios, where the start and end boundaries of actions (e.g., a forehand shot) can be visually ambiguous and difficult to define precisely [46].

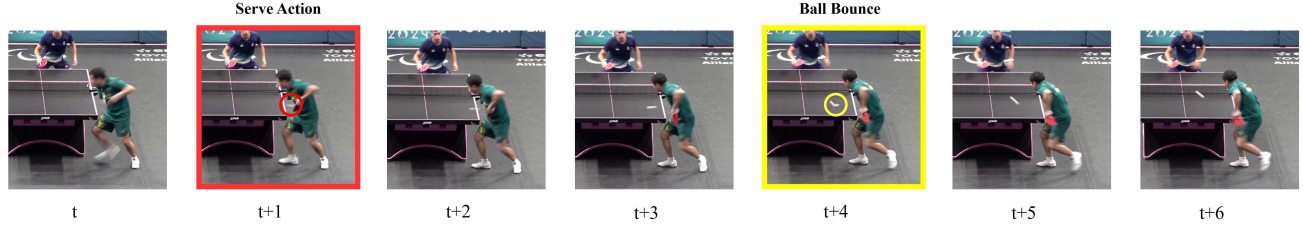


Figure 1. Example of Precise Event Spotting in table tennis: the exact moments when the player contacts the ball during a serve (highlighted in red) and when the ball bounces on the table (highlighted in yellow). The ball locations are circled accordingly. t represents the timestamp at the frame level.

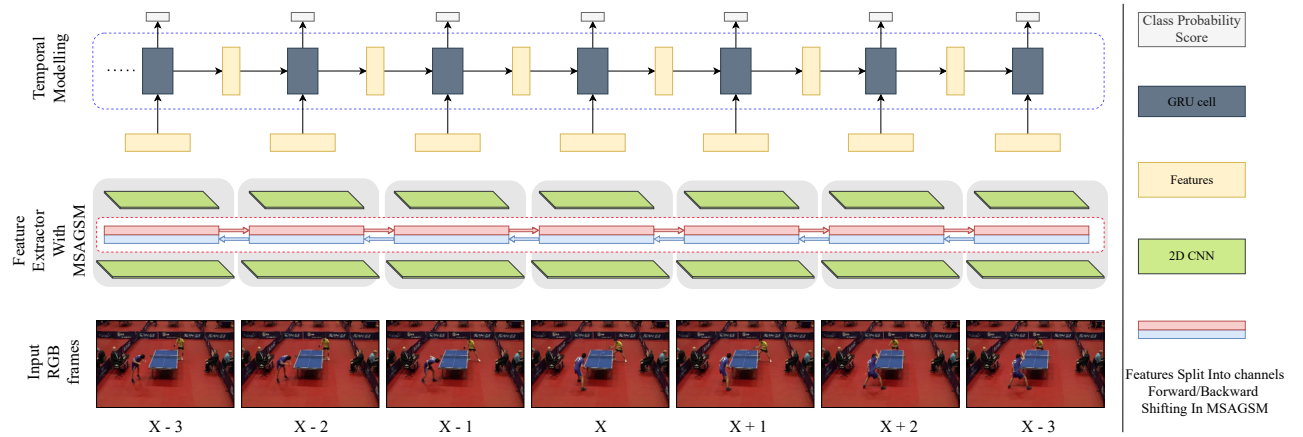


Figure 2. Overview of our proposed architecture for Precise Event Spotting. The input video is processed through a 2D CNN backbone for spatial feature extraction, followed by the Multi-Scale Attention Gate Shift Module (MSAGSM) for spatio-temporal modeling. MSAGSM combines channel-group spatial attention and multi-scale temporal shifting to capture varying temporal dependencies. The resulting features are passed through a GRU-based temporal model to predict event class probabilities at the frame level.

To address this ambiguity, the SoccerNet dataset introduced the task of Action Spotting [9], which focuses on identifying key frames of important events within a relaxed temporal window (e.g., ± 50 frames). Subsequently, PES was proposed to enforce a stricter temporal tolerance, requiring models to be accurate within just a few frames.

E2E-Spot [12] serves as a strong PES baseline, combining RegNetY [25] with the Gate Shift Module (GSM) [31] for temporal modeling. Building on this, T-DEED [44] addressed the challenge of distinguishing between adjacent frames with highly similar visual appearance by incorporating the Scalable Granularity Perception module [29] to enhance discriminability among temporally close features. UGLF [37] takes a different direction by integrating the vision-language model GLIP [16], marking the first use of vision-language features for PES. Most recently, ASTRM [27] further advanced the field by improving long-range temporal dependency through spatial-temporal feature injection into the feature extractor and proposing the Soft Instance Contrastive (SoftIC) loss to mitigate class imbalance.

Beyond visual features, audio signals can also serve as important cues in sports, for instance, crowd noise after a goal. ASTRA [43], a transformer-based encoder-decoder model designed for soccer, integrates both visual and audio embeddings, using learnable queries in the decoder to jointly attend to multi-modal cues.

Other Sports Video Tasks: Ball tracking methods such as the TrackNet family [4, 13, 19, 26, 33, 47] focus on recovering ball trajectories, with TrackNetV4 introducing motion-aware attention maps from frame differences. While related, tracking localizes objects whereas PES targets the timing and semantics of fine-grained events. These approaches are thus complementary, and accurate trajectories could provide useful cues for future event detection.

Sports Video Datasets: Existing PES datasets are often acquired from broadcast videos from high-level matches such as [9, 11, 12, 28, 48]. These datasets are fine-grained, where all event and class labels relate to a single activity. Other sports-related video datasets include ball tracking [13, 33, 34, 47] and sports video captioning [23, 42, 49, 51].

Despite progress, PES methods still struggle to capture long-range temporal dependencies while attending to fine-grained spatial cues. In addition, most datasets rely on broadcast footage with fixed cameras and ideal conditions, which overlook the challenges of community-level sports. To bridge these gaps, we propose MSAGSM, a lightweight block for enhanced temporal reasoning and spatial focus, and introduce TTA, the first table tennis PES benchmark with consumer-grade courtside videos featuring variable viewpoints, camera motion, and frequent occlusions.

3. Multi-Scale Attention GSM

3.1. Model Overview

Figure 2 illustrates an overview of our proposed MSAGSM architecture. It enables 2D CNNs to capture varying spatio-temporal dependencies through an efficient combination of multi-scale gated shifting and channel-group spatial attention mechanisms. The proposed method consists of two main components: (1) a multi-head channel-grouped spatial attention module, which splits the input features into multiple groups and applies attention independently to each group, allowing the model to focus on spatially informative regions; and (2) a multi-scale GSM, which introduces multiscale temporal dilations to shift features across varying temporal distances. This design allows the model to directly access a broader temporal context compared to the original GSM.

3.2. Channel Grouped Spatial Attention

Our intuition is rooted in the observation that, in sports videos, most critical events are concentrated around key entities such as players, referees, and the ball. In contrast, a large portion of each frame consists of background content that contributes little to event detection. Motivated by the effectiveness of attention mechanisms in prior work [3, 6, 40, 41], we extend the original GSM into a **channel-grouped spatial attention GSM**. This design allows the model to focus on spatially informative regions while suppressing irrelevant background, thereby improving the accuracy of event spotting. Figure 3 shows the details of the channel-grouped spatial attention mechanism.

We generate spatial attention maps using 2D convolutional layers to highlight the most informative regions within a feature map. Given an intermediate feature tensor, we first split it into multiple groups along the channel dimension, where the number of groups corresponds to a predefined number of attention heads—a tunable hyperparameter.

The motivation behind using multiple spatial attention heads is to account for the varying number of salient regions required across different sports. For example, in tennis, the model must simultaneously attend to multiple entities such

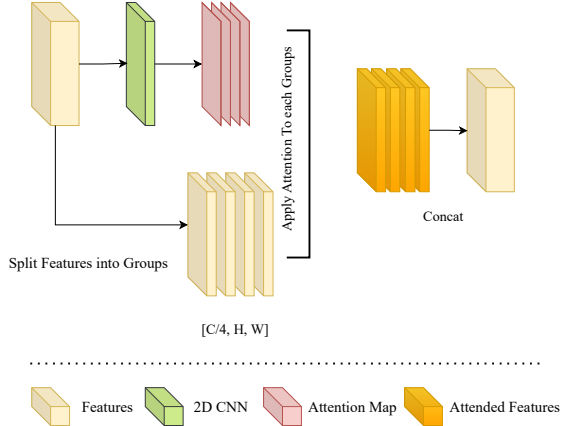


Figure 3. Illustration of the spatial attention mechanism in the proposed MSAGSM module. Feature maps from the 2D CNN are divided into multiple channel-wise chunks (e.g., $C/4$ per group). Each chunk is processed independently through a spatial attention module to highlight relevant regions (e.g., players, ball) while suppressing background noise. The attended features are then concatenated and forwarded to the temporal modeling block.

as two players and a fast-moving ball, whereas in diving, the focus is typically on a single athlete. Conventional spatial attention mechanisms produce a single attention map, which limits the model’s capacity to flexibly adapt to such variation. In contrast, our multi-head design enables the model to learn multiple independent attention maps, allowing it to focus on different regions as needed, and offering greater flexibility and expressiveness across diverse sporting contexts.

For each head, a 2D convolutional layer generates a spatial attention map based on the original features. These maps are applied independently to their corresponding feature chunks, allowing each head to specialize in distinct spatial regions in a data-driven manner. Finally, the attended feature chunks are concatenated to reconstruct a unified refined feature representation.

3.3. Multi-Scale GSM

We adopt the GSM as a reference architecture, as it has been proven effective in the PES domain [12, 37, 44]. GSM performs a gating-based temporal shifting mechanism inspired by TSM [17] and GST [22]. However, a key limitation of GSM is that it only performs shifts across adjacent frames, restricting its ability to capture longer range temporal dependencies directly, which is often important in sports videos to classify events and discriminate similar frames.

We propose the MSAGSM, which extends GSM by replacing fixed, adjacent frame shifting with a learnable spatially aware gating mechanism that enables direct access to longer temporal ranges. The architectural design of

MSAGSM is illustrated in Figure 4.

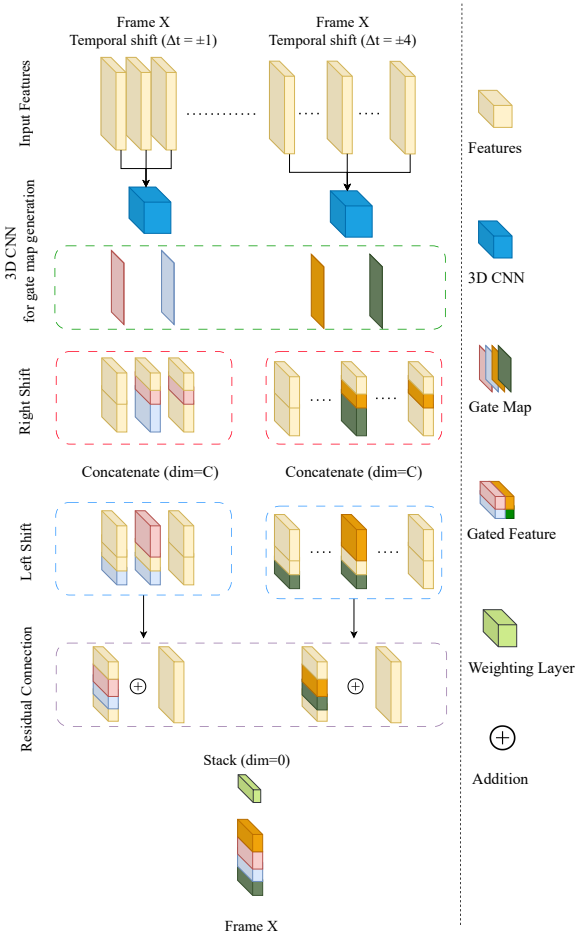


Figure 4. Structure of the proposed Multi-Scale Gate Shift Module. Given input features, a 3D CNN generates gate maps corresponding to different temporal shift ranges (e.g., $\Delta t = \pm 1, \pm 4$). Features are shifted left and right across multiple scales, gated accordingly, and combined through concatenation and stacking. This design enables the model to adaptively capture both short and long-term temporal dependencies in a data-driven manner, while preserving the original information.

Given a sequence of feature maps $X \in \mathbb{R}^{C \times T \times H \times W}$, where C is the number of channels, T is the temporal length, and H and W denote the height and width of a frame, respectively. For each temporal distance scale, MSAGSM first applies a gating layer implemented as a 3D CNN. This gating layer receives a temporal window of three feature maps sampled across time centered around the current timestamp. Two gating maps, corresponding to the left and right shifts, are generated for each feature map. These gates are passed through the \tanh activation function to constrain their values to the range $(-1, +1)$, ensuring sta-

ble modulation:

$$(G_{\text{left}}, G_{\text{right}}) = \tanh(\text{Conv3D}(X)). \quad (1)$$

The feature map is split into two groups, $X = [X_{\text{left}}, X_{\text{right}}]$, each multiplied element-wise by its corresponding gate map and then temporally shifted left or right via a rolling operation:

$$\hat{X}_{\text{left}} = \text{Roll}(X_{\text{left}} \odot G_{\text{left}}, -\delta), \quad (2)$$

$$\hat{X}_{\text{right}} = \text{Roll}(X_{\text{right}} \odot G_{\text{right}}, +\delta). \quad (3)$$

Here, \odot denotes element-wise multiplication, and δ is the temporal shift distance (in frames).

Padding is applied to maintain shape integrity and prevent feature loss at the sequence boundaries. To preserve important information, the shifted features are added back to the original input via a residual connection. The gated, shifted features are then concatenated along the channel dimension to restore the original shape,

$$\hat{X} = [\hat{X}_{\text{left}}, \hat{X}_{\text{right}}] + X. \quad (4)$$

Finally, the outputs from different distance levels are stacked along a new dimension and passed through a learnable weighting mechanism. This layer adaptively determines the importance of each temporal scale, enabling the model to incorporate information across varying temporal distances. Formally, let $\{\hat{X}^{(i)}\}_{i=1}^N$ denote the outputs from N different shift ranges. The final output is computed as:

$$\hat{X}_{\text{final}} = \sum_{i=1}^N w_i \cdot \hat{X}^{(i)}, \quad \text{where } \sum_{i=1}^N w_i = 1, w_i \geq 0. \quad (5)$$

Here, w_i are learnable scalar weights normalized via a softmax function. This design allows the model to emphasize the most relevant temporal scales while introducing only minimal computational overhead compared to the original GSM.

4. Empirical Study

In this section, we describe the datasets (with details on the new TTA dataset), outline implementation settings, present ablation studies, and compare MSAGSM with prior methods and state-of-the-art baselines.

4.1. Datasets

We evaluate our method on four fine-grained sports video datasets with frame-level annotations: Tennis [53], Figure Skating [11], FineDiving [48], and our proposed TTA dataset.

The Tennis dataset consists of 3,345 video clips from 28 matches, with frame rates of 25 or 30 FPS. It contains 33,791 frame-accurate annotations spanning six event

Examples of TTA Dataset



Figure 5. Example frames from the proposed TTA dataset. The top row shows samples from World Para Future matches, while the bottom row displays clips from the 2024 Paris Paralympic Games. The dataset captures diverse viewing angles, frequent occlusions, and high event density, representative of real-world table tennis matches.

classes. The Figure Skating dataset includes 11 broadcast videos (all 25 FPS), covering 371 short program performances from major international competitions between 2010 and 2019. It includes 3,674 annotated events across four classes. Following previous work [11, 37, 44], we adopt two evaluation splits: a competition split (FS-Comp) and a performance split (FS-Perf). The FineDiving dataset comprises 3,000 diving clips with temporal segment annotations, totaling 7,010 events. These have been converted into frame-level event labels across four classes using the annotation protocol from [12].

We also introduce the Table Tennis Australia (TTA) dataset details shown in Table 1, the first PES benchmark for table tennis. It consists of 39 full-game videos recorded at 30 FPS, totaling 4,878 annotated events across 8 classes: serve, bounce, forehand, and backhand, each labeled separately for near and far sides of the table. Examples of the TTA dataset are presented in Figure 5. Events are annotated following labeling protocols from Table Tennis Australia. For example, a frame is labeled as an event when the ball contacts the paddle or undergoes significant motion immediately after. In cases of occlusion (e.g., when a player blocks the ball near the camera), temporal context from preceding and following frames is used to estimate the most accurate event frame. For more details, please refer to the **Supp. §2**.

Unlike existing datasets, TTA videos are collected using handheld cameras by professional analysts from Paralympics Australia. The dataset includes elite level competitions such as the Paralympics and World Para Future. This real-world, single camera setting introduces challenges such as frequent occlusions, motion blur, and dynamic an-

Table 1. Comparison of PES benchmark datasets. TTA (**Bold**) offers higher event density and realistic recording conditions.

Dataset	Recording	Events	Classes	Density
TTA (Ours)	Handheld	4,878	8	7.73
Tennis	Broadcast	33,791	6	3.81
Figure Skating	Broadcast	3,674	4	1.58
FineDiving	Broadcast	7010	4	1.49

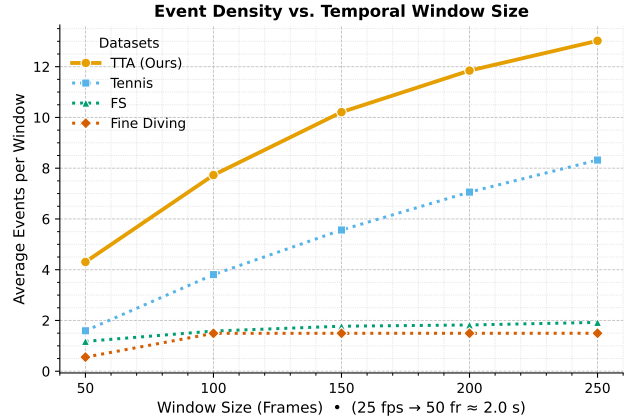


Figure 6. Comparison of event density (average number of events) across varying temporal window sizes. TTA shows the highest event density across all ranges, reflecting its fine-grained and fast-paced nature.

gles—conditions closer to practical applications—unlike the broadcast quality videos used in most prior work. As shown in Figure 6, TTA exhibits the highest event density among all datasets, averaging 7.73 events per 100 frame window, compared to 3.81 in Tennis and significantly fewer in others. This emphasizes the need for models that can capture fine-grained temporal structure and distinguish between visually similar frames within narrow time intervals.

4.2. Evaluation

Since our proposed module, MSAGSM, is designed to be a lightweight and drop in replacement for GSM, we follow the same training procedure as the E2E-Spot baseline [12], replacing GSM with MSAGSM in the backbone. The model performance is evaluated using the mean Average Precision (mAP), computed by averaging the Average Precision across all event classes. We report mAP under $\delta \in \{0, 1, 2\}$, where $\delta = 0$ requires an exact-frame match and $\delta = 1/2$ allow a $\pm 1/ \pm 2$ -frame tolerance.

4.3. Implementation Details

We closely follow the training protocol of E2E-Spot [12], adopting its default configurations for a fair comparison. Specifically, all models are trained with input clips of length

Table 2. Performance comparison (mAP %) at different temporal tolerances ($\delta = 0, 1, 2$) across five fine-grained sports video datasets. The best result in each column is shown in **bold**, and our proposed method is *italicized*. A \star marks the best result within each model–backbone group. All models are evaluated with a fixed clip length of 100 frames.

Model	Temp	TTA			Tennis			FS_Comp			FS_Perf			FineDiving			P (M) / GFLOPs
		$\delta=0$	$\delta=1$	$\delta=2$	$\delta=0$	$\delta=1$	$\delta=2$	$\delta=0$	$\delta=1$	$\delta=2$	$\delta=0$	$\delta=1$	$\delta=2$	$\delta=0$	$\delta=1$	$\delta=2$	
ASTRA[43]	-	28.12	54.16	60.95	49.98	88.67	97.49	35.87	73.45	84.71	39.35	78.10	90.05	27.28	65.01	82.74	4.49 / 42.20
ASFormer[50]	-	21.68	40.69	61.08	42.57	89.34	93.39	32.60	50.29	55.97	16.34	36.46	58.41	15.86	66.82	87.11	3.21 / 41.94
E2E-Spot[12]	GSM	34.36	66.42	76.90	51.42	90.03	96.48	36.44	75.39	89.33	39.32	81.27	94.14	27.31	67.89	86.97	4.45 / 42.18
E2E-Spot	GSF	36.17	63.70	72.19	49.68	89.01	96.55*	36.25	75.49	89.32	40.07	81.55	94.02	29.41	67.57	86.22	4.45 / 42.20
<i>E2E-Spot</i>	<i>Ours</i>	36.43*	69.50*	78.12*	55.51*	91.34*	96.51	38.34*	77.72*	90.04*	46.54*	84.12*	96.90*	29.83*	71.03*	87.26*	4.51 / 45.06
T-DEED	GSM	33.32*	60.69	69.30	48.82	89.21	97.15*	38.61	71.69	90.02	42.53	79.62	90.36	26.86	66.18	84.02	16.42 / 43.34
T-DEED[44]	GSF	26.27	54.04	64.51	50.08	89.58	97.06	38.83	75.52	92.15*	38.89	79.82	94.79*	28.50	67.04*	83.24	16.42 / 43.34
<i>T-DEED</i>	<i>Ours</i>	28.06	60.77*	72.50*	52.76*	90.68*	96.67	39.06*	75.55*	87.61	44.66*	82.41*	94.12	26.88*	66.70	84.60*	16.48 / 46.20
UGLF[37]	GSM	34.36	63.52	71.16	50.31	89.73	97.16*	36.99	77.25	90.44	38.29	79.24	93.08	27.11	66.88	84.94	4.45 / 42.18
UGLF	GSF	36.17*	63.70	72.19	50.94	89.39	97.06	34.84	72.61	86.90	37.41	82.06	94.38	29.81	66.65	84.27	4.45 / 42.20
<i>UGLF</i>	<i>Ours</i>	33.93	64.82*	74.84*	53.10*	90.98*	97.10	39.66*	78.86*	91.13*	46.59*	82.64*	96.12*	29.59*	67.21*	85.34*	4.51 / 45.06

$L = 100$ frames, a batch size of 8, and 5,000 randomly sampled clips per epoch. Training runs for 50 epochs using the AdamW optimizer [21] with a base learning rate of 1×10^{-3} , 3 warm-up epochs, and a cosine decay schedule. As in E2E-Spot, positive classes in the cross-entropy loss are weighted by $w = 5$ to handle class imbalance. We also adopt the same backbones—RegNetY-200 [25] and ResNet-18 [10]—from the original framework. Unless otherwise noted, all experiments are conducted on a single NVIDIA L40S GPU.

4.4. Comparison with State-of-the-Art

To evaluate MSAGSM, we compare against five representative PES models. ASTRA [43] and ASFormer [50] serve as Transformer baselines, while E2E-Spot [12], T-DEED [44], and UGLF [37] are CNN-based methods combining a 2D backbone, temporal module, and decoder. E2E-Spot and UGLF both employ GSM [31], whereas T-DEED adopts GSF [32].

For CNN-based methods, we test both the original temporal module and a drop-in replacement with our MSAGSM, and we also compare different temporal modules within the same backbone–decoder setup. All models are trained from official codebases under identical conditions.

Main Results. Table 2 presents results on five fine-grained sports video datasets under three temporal tolerance thresholds ($\delta = 0, \delta = 1, \delta = 2$). Across the board, our proposed MSAGSM module consistently outperforms existing temporal modeling approaches. For example, within the E2E-Spot architecture using RegNetY-200 [25], MSAGSM improves upon GSM by **+4.09** mAP on Tennis at $\delta = 0$, by **+3.08** mAP on TTA at $\delta = 1$, and by **+3.14** mAP on Fine-Diving at $\delta = 1$. Similar performance gains are observed

when MSAGSM replaces the original temporal module in more complex models such as T-DEED and UGLF.

Out of all possible comparisons across model backbone configurations, MSAGSM achieves the best result in **37 out of 45** cases when compared directly against other temporal modules. Furthermore, it ranks first in **13 out of 15** columns when considering overall best scores, setting new SOTA performance simply by replacing the temporal component.

Backbone and Module Versatility. To evaluate the generality of our approach, we further experiment with alternative backbones, specifically ResNet-18 [10] in E2E-Spot, T-DEED, and UGLF architectures. For simplicity, the main table includes RegNetY-200 results only, while additional results with ResNet-18 [10] are provided in the **Supp. §3.1**. For both E2E-Spot and UGLF, which use relatively simple temporal modules, our MSAGSM yields substantial gains with minimal complexity overhead, achieving the best performance in **14/15** and **13/15** evaluation groups, respectively. The improvement is less pronounced for T-DEED, which already employs a more sophisticated temporal design. In this case, adding MSAGSM may introduce redundant or overlapping temporal cues, making feature aggregation less effective.

Efficiency. MSAGSM remains lightweight, requiring only **4.5M** parameters and **45.06 GFLOPs** in its default setting. This is comparable to existing temporal modules and only slightly larger in size, yet it consistently delivers higher accuracy. Its compact design makes MSAGSM a practical drop-in replacement for both lightweight and large-scale models built on 2D pretrained CNN backbones.

Summary. These results demonstrate the effectiveness of MSAGSM as a robust and efficient temporal modeling module. Its consistent improvements across diverse mod-

Table 3. Ablation study on attention head count, temporal distance range, and clip length using the MSAGSM module on the TTA dataset. All results are reported in mAP (%), default clip length=100, best result is in bold.

Setting	Value	$\delta = 1$	$\delta = 2$	P(M) / GFLOPs
<i>MSAGSM w/o Attention</i>				
E2E-GSM	-	66.42	76.90	4.45 / 42.18
Distance	[1,2]	66.08	77.31	4.47 / 43.26
Distance	[1,2,3]	65.82	74.67	4.49 / 44.32
Distance	[1,2,3,4]	64.39	74.91	4.51 / 45.40
<i>GSM with Channel Group Spatial Attention</i>				
E2E-GSM	-	66.42	76.90	4.45 / 42.18
Heads	1	67.02	75.74	4.46 / 42.56
Heads	2	65.39	72.35	4.47 / 42.92
Heads	3	64.01	71.94	4.47 / 43.28
<i>Varying Number of Attention Heads (Distance = [1,2,3])</i>				
Heads	1	60.99	75.38	4.50 / 44.68
Heads	2	69.50	78.12	4.51 / 45.06
Heads	3	65.87	75.87	4.51 / 45.42
Heads	4	61.01	72.98	4.52 / 45.78
<i>Varying Temporal Window Size (Heads = 2)</i>				
Distance	[1,2]	60.78	71.10	4.48 / 43.98
Distance	[1,2,3]	69.50	78.12	4.51 / 45.06
Distance	[1-4]	64.18	71.59	4.53 / 46.12
Distance	[1-5]	67.54	67.41	4.55 / 47.18
Distance	[1-6]	64.03	75.38	4.57 / 48.26
<i>Varying Clip Length with Distance=[1,2,3], Heads=2</i>				
Length	25	56.34	64.85	4.47 / 10.72
Length	50	58.56	66.80	4.47 / 21.46
Length	100	69.50	78.12	4.47 / 47.52
Length	150	62.24	74.50	4.47 / 64.22
Length	200	57.29	66.78	4.47 / 85.50

els and baseline temporal modules, particularly on our proposed **TTA** benchmark, underscore its suitability for capturing the high-frequency, fine-grained temporal dynamics inherent in sports video understanding.

4.5. Ablation Study

We conduct ablation studies on the **TTA** and **FineDiv-ing** datasets, which represent two contrasting types of sports—one with high event density and the other with sparse events.

Isolating Components. We evaluate the effectiveness of our proposed extensions to GSM by isolating them individually. First, we test the multi-scale GSM with different temporal distance ranges. As shown in Table 3, increasing the range alone leads to inconsistent performance, since exchanging more temporal information without guidance can introduce noise. Next, we assess the channel-group spatial attention GSM by applying different numbers of attention heads to the baseline E2E-GSM. A single head provides

a slight gain by directing focus to the most salient region, but additional heads do not yield consistent improvements. This suggests that attention alone lacks sufficient temporal context to fully exploit multiple regions of interest.

Finally, when combining both components, their individual limitations are mitigated: channel-group spatial attention highlights the most informative regions, while multi-scale shifts propagate this focused information across time. Together, they form MSAGSM, which consistently outperforms the baseline.

Attention Heads and Temporal Window Size. We study the effect of varying attention heads (with distance fixed at [1, 2, 3]) and dilation ranges (with heads fixed at two). On TTA, increasing the number of heads from one to two substantially improves mAP (+8.51 and +2.74 at $\delta = 1, 2$), but adding more heads leads to inconsistent or reduced performance, likely due to over-fragmentation.

For distance ranges, the default [1, 2, 3] provides the strongest and most stable results. Slight gains are seen with [1, 2, 3, 4], but very large windows (e.g., [1, ..., 6]) dilute fine-grained cues and hurt stability. Overall, while optimal hyperparameters may vary slightly with dataset characteristics, two attention heads and a temporal window of [1, 2, 3] yield the most consistent performance across benchmarks on the validation sets. All results in the main tables are reported using these default settings, with further ablations including validations are provided in the [Supp. §3.3](#).

Clip length. We also examine the impact of clip length. As shown in Table 3, a length of 100 frames achieves the best performance, which is consistent with prior findings in [12].

5. Limitations and Future Work

MSAGSM enables rich temporal modeling with minimal overhead, making it a practical choice for real-world applications. We observe that it performs particularly well with both strong backbones and lightweight models, suggesting that better feature representations further amplify its effectiveness.

Although our work focuses on PES, MSAGSM could also benefit broader video understanding tasks such as action recognition, where sparse frame sampling limits temporal precision. Future work may explore how fine-grained modules like MSAGSM can bridge this gap.

We acknowledge two key limitations. First, MSAGSM is sensitive to hyperparameters (e.g., temporal distance, attention heads), requiring dataset-specific tuning and reducing plug-and-play generalization across datasets. Second, per-class precision-recall analysis on TTA ([Supp. §3.6](#)) shows frequent confusion between forearm and backhand strokes due to their visual similarity and player handedness, whereas distinct events like bounces are recognized more reliably.

Future directions include adaptive strategies for automatically learning temporal distances and methods to better handle fine-grained ambiguities and viewpoint variations.

6. Conclusion

We propose **MSAGSM**, a lightweight temporal module for 2D backbones that combines temporal shifts and attention. Across five fine-grained PES datasets, it consistently improves performance, boosting mAP@0 by **+4.09** and mAP@1 by **+3.08%** on TTA with only **0.01M** extra parameters. We also present **TTA**, a new table tennis PES benchmark with realistic recordings and high event density, to support future research in fine-grained sports video understanding.

References

[1] Mengqi Cao, Min Yang, Guozhen Zhang, Xiaotian Li, Yilu Wu, Gangshan Wu, and Limin Wang. Spotformer: A transformer-based framework for precise soccer action spotting. In *2022 IEEE 24th International Workshop on Multimedia Signal Processing (MMSP)*, pages 1–6. IEEE, 2022. 1

[2] Bo Chen, Fangzhou Meng, Hongying Tang, and Guanjun Tong. Two-level attention module based on spurious-3d residual networks for human action recognition. *Sensors*, 23(3):1707, 2023. 2

[3] Long Chen, Hanwang Zhang, Jun Xiao, Liqiang Nie, Jian Shao, Wei Liu, and Tat-Seng Chua. Sca-cnn: Spatial and channel-wise attention in convolutional networks for image captioning. In *Proceedings of the IEEE conference on computer vision and pattern recognition*, pages 5659–5667, 2017. 4

[4] Yu-Jou Chen and Yu-Shuen Wang. Tracknetv3: Enhancing shuttlecock tracking with augmentations and trajectory rectification. In *Proceedings of the 5th ACM International Conference on Multimedia in Asia*, pages 1–7, 2023. 3

[5] Julien Denize, Mykola Liashuhu, Jaonary Rabarisoa, Astrid Orcesi, and Romain Héault. Comedian: Self-supervised learning and knowledge distillation for action spotting using transformers. In *Proceedings of the IEEE/CVF Winter Conference on Applications of Computer Vision*, pages 530–540, 2024. 1

[6] Alexey Dosovitskiy, Lucas Beyer, Alexander Kolesnikov, Dirk Weissenborn, Xiaohua Zhai, Thomas Unterthiner, Mostafa Dehghani, Matthias Minderer, Georg Heigold, Sylvain Gelly, et al. An image is worth 16x16 words: Transformers for image recognition at scale. *arXiv preprint arXiv:2010.11929*, 2020. 2, 4

[7] Haoqi Fan, Bo Xiong, Karttikeya Mangalam, Yanghao Li, Zhicheng Yan, Jitendra Malik, and Christoph Feichtenhofer. Multiscale vision transformers. In *Proceedings of the IEEE/CVF international conference on computer vision*, pages 6824–6835, 2021. 2

[8] Christoph Feichtenhofer, Haoqi Fan, Jitendra Malik, and Kaiming He. Slowfast networks for video recognition. In *Proceedings of the IEEE/CVF international conference on computer vision*, pages 6202–6211, 2019. 2

[9] Silvio Giancola, Mohieddine Amine, Tarek Dghaily, and Bernard Ghanem. Soccernet: A scalable dataset for action spotting in soccer videos. In *Proceedings of the IEEE conference on computer vision and pattern recognition workshops*, pages 1711–1721, 2018. 2, 3

[10] Kaiming He, Xiangyu Zhang, Shaoqing Ren, and Jian Sun. Deep residual learning for image recognition. In *Proceedings of the IEEE conference on computer vision and pattern recognition*, pages 770–778, 2016. 7, 12

[11] James Hong, Matthew Fisher, Michaël Gharbi, and Kayvon Fatahalian. Video pose distillation for few-shot, fine-grained sports action recognition. In *Proceedings of the IEEE/CVF International Conference on Computer Vision*, pages 9254–9263, 2021. 2, 3, 5, 6

[12] James Hong, Haotian Zhang, Michaël Gharbi, Matthew Fisher, and Kayvon Fatahalian. Spotting temporally precise, fine-grained events in video. In *European Conference on Computer Vision*, pages 33–51. Springer, 2022. 1, 2, 3, 4, 6, 7, 8, 12, 14

[13] Yu-Chuan Huang, I-No Liao, Ching-Hsuan Chen, Tsì-Uí Ík, and Wen-Chih Peng. Tracknet: A deep learning network for tracking high-speed and tiny objects in sports applications. In *2019 16th IEEE International Conference on Advanced Video and Signal Based Surveillance (AVSS)*, pages 1–8. IEEE, 2019. 3

[14] Boyuan Jiang, MengMeng Wang, Weihao Gan, Wei Wu, and Junjie Yan. Stm: Spatiotemporal and motion encoding for action recognition. In *Proceedings of the IEEE/CVF international conference on computer vision*, pages 2000–2009, 2019. 2

[15] Dan Kondratyuk, Liangzhe Yuan, Yandong Li, Li Zhang, Mingxing Tan, Matthew Brown, and Boqing Gong. Movinets: Mobile video networks for efficient video recognition. In *Proceedings of the IEEE/CVF conference on computer vision and pattern recognition*, pages 16020–16030, 2021. 2

[16] Liunian Harold Li, Pengchuan Zhang, Haotian Zhang, Jianwei Yang, Chunyuan Li, Yiwu Zhong, Lijuan Wang, Lu Yuan, Lei Zhang, Jenq-Neng Hwang, et al. Grounded language-image pre-training. In *Proceedings of the IEEE/CVF conference on computer vision and pattern recognition*, pages 10965–10975, 2022. 3

[17] Ji Lin, Chuang Gan, and Song Han. Tsm: Temporal shift module for efficient video understanding. In *Proceedings of the IEEE/CVF international conference on computer vision*, pages 7083–7093, 2019. 2, 4

[18] Tianwei Lin, Xu Zhao, Haisheng Su, Chongjing Wang, and Ming Yang. Bsn: Boundary sensitive network for temporal action proposal generation. In *Proceedings of the European conference on computer vision (ECCV)*, pages 3–19, 2018. 2

[19] Paul Liu and Jui-Hsien Wang. Monotrack: Shuttle trajectory reconstruction from monocular badminton video. In *Proceedings of the IEEE/CVF Conference on Computer Vision and Pattern Recognition*, pages 3513–3522, 2022. 3

[20] Ze Liu, Jia Ning, Yue Cao, Yixuan Wei, Zheng Zhang, Stephen Lin, and Han Hu. Video swin transformer. In *Proceedings of the IEEE/CVF international conference on computer vision*, pages 6202–6211, 2019. 2

ceedings of the IEEE/CVF conference on computer vision and pattern recognition, pages 3202–3211, 2022. 2

[21] Ilya Loshchilov and Frank Hutter. Decoupled weight decay regularization. *arXiv preprint arXiv:1711.05101*, 2017. 7

[22] Chenxu Luo and Alan L Yuille. Grouped spatial-temporal aggregation for efficient action recognition. In *Proceedings of the IEEE/CVF international conference on computer vision*, pages 5512–5521, 2019. 2, 4

[23] Mengshi Qi, Yunhong Wang, Annan Li, and Jiebo Luo. Sports video captioning via attentive motion representation and group relationship modeling. *IEEE Transactions on Circuits and Systems for Video Technology*, 30(8):2617–2633, 2019. 3

[24] Zhaofan Qiu, Ting Yao, and Tao Mei. Learning spatio-temporal representation with pseudo-3d residual networks. In *proceedings of the IEEE International Conference on Computer Vision*, pages 5533–5541, 2017. 2

[25] Ilija Radosavovic, Raj Prateek Kosaraju, Ross Girshick, Kaiming He, and Piotr Dollár. Designing network design spaces. In *Proceedings of the IEEE/CVF conference on computer vision and pattern recognition*, pages 10428–10436, 2020. 3, 7, 12

[26] Arjun Raj, Lei Wang, and Tom Gedeon. Tracknetv4: Enhancing fast sports object tracking with motion attention maps. In *ICASSP 2025-2025 IEEE International Conference on Acoustics, Speech and Signal Processing (ICASSP)*, pages 1–5. IEEE, 2025. 3

[27] Sanchayan Santra, Vishal Chudasama, Pankaj Wasnik, and Vineeth N Balasubramanian. Precise event spotting in sports videos: Solving long-range dependency and class imbalance. In *Proceedings of the Computer Vision and Pattern Recognition Conference*, pages 3163–3172, 2025. 1, 3, 12

[28] Dian Shao, Yue Zhao, Bo Dai, and Dahua Lin. Finegym: A hierarchical video dataset for fine-grained action understanding. In *Proceedings of the IEEE/CVF conference on computer vision and pattern recognition*, pages 2616–2625, 2020. 2, 3

[29] Dingfeng Shi, Yujie Zhong, Qiong Cao, Lin Ma, Jia Li, and Dacheng Tao. Tridet: Temporal action detection with relative boundary modeling. In *Proceedings of the IEEE/CVF Conference on Computer Vision and Pattern Recognition*, pages 18857–18866, 2023. 3

[30] Haisheng Su, Weihao Gan, Wei Wu, Yu Qiao, and Junjie Yan. Bsn++: Complementary boundary regressor with scale-balanced relation modeling for temporal action proposal generation. In *Proceedings of the AAAI conference on artificial intelligence*, pages 2602–2610, 2021. 2

[31] Swathikiran Sudhakaran, Sergio Escalera, and Oswald Lanz. Gate-shift networks for video action recognition. In *Proceedings of the IEEE/CVF conference on computer vision and pattern recognition*, pages 1102–1111, 2020. 1, 2, 3, 7

[32] Swathikiran Sudhakaran, Sergio Escalera, and Oswald Lanz. Gate-shift-fuse for video action recognition. *IEEE Transactions on Pattern Analysis and Machine Intelligence*, 45(9):10913–10928, 2023. 2, 7

[33] Nien-En Sun, Yu-Ching Lin, Shao-Ping Chuang, Tzu-Han Hsu, Dung-Ru Yu, Ho-Yi Chung, and Tsui-Uí Ík. Tracknetv2: Efficient shuttlecock tracking network. In *2020 International Conference on Pervasive Artificial Intelligence (ICPAI)*, pages 86–91. IEEE, 2020. 3

[34] Shuhei Tarashima, Muhammad Abdul Haq, Yushan Wang, and Norio Tagawa. Widely applicable strong baseline for sports ball detection and tracking. In *BMVC*, 2023. 3

[35] Zhan Tong, Yibing Song, Jue Wang, and Limin Wang. Videomae: Masked autoencoders are data-efficient learners for self-supervised video pre-training. *Advances in neural information processing systems*, 35:10078–10093, 2022. 2

[36] Du Tran, Heng Wang, Lorenzo Torresani, Jamie Ray, Yann LeCun, and Manohar Paluri. A closer look at spatiotemporal convolutions for action recognition. In *Proceedings of the IEEE conference on Computer Vision and Pattern Recognition*, pages 6450–6459, 2018. 2

[37] Kim Hoang Tran, Phuc Vuong Do, Ngoc Quoc Ly, and Ngan Le. Unifying global and local scene entities modelling for precise action spotting. In *2024 International Joint Conference on Neural Networks (IJCNN)*, pages 1–8. IEEE, 2024. 1, 3, 4, 6, 7, 12, 14

[38] Bastien Vanderplas and Stephane Dupont. Improved soccer action spotting using both audio and video streams. In *Proceedings of the IEEE/CVF Conference on Computer Vision and Pattern Recognition Workshops*, pages 896–897, 2020. 1

[39] Limin Wang, Yuanjun Xiong, Zhe Wang, Yu Qiao, Dahua Lin, Xiaou Tang, and Luc Van Gool. Temporal segment networks: Towards good practices for deep action recognition. In *European conference on computer vision*, pages 20–36. Springer, 2016. 2

[40] Qilong Wang, Banggu Wu, Pengfei Zhu, Peihua Li, Wangmeng Zuo, and Qinghua Hu. Eca-net: Efficient channel attention for deep convolutional neural networks. In *Proceedings of the IEEE/CVF conference on computer vision and pattern recognition*, pages 11534–11542, 2020. 4

[41] Sanghyun Woo, Jongchan Park, Joon-Young Lee, and In So Kweon. Cbam: Convolutional block attention module. In *Proceedings of the European conference on computer vision (ECCV)*, pages 3–19, 2018. 4

[42] Dekun Wu, He Zhao, Xingce Bao, and Richard P Wildes. Sports video analysis on large-scale data. In *European conference on computer vision*, pages 19–36. Springer, 2022. 3

[43] Artur Xarles, Sergio Escalera, Thomas B Moeslund, and Albert Clapés. Astra: An action spotting transformer for soccer videos. In *Proceedings of the 6th International Workshop on Multimedia Content Analysis in Sports*, pages 93–102, 2023. 1, 3, 7, 12

[44] Artur Xarles, Sergio Escalera, Thomas B Moeslund, and Albert Clapés. T-deed: Temporal-discriminability enhancer encoder-decoder for precise event spotting in sports videos. In *Proceedings of the IEEE/CVF Conference on Computer Vision and Pattern Recognition*, pages 3410–3419, 2024. 1, 2, 3, 4, 6, 7, 12, 14

[45] Saining Xie, Chen Sun, Jonathan Huang, Zhuowen Tu, and Kevin Murphy. Rethinking spatiotemporal feature learning: Speed-accuracy trade-offs in video classification. In *Proceedings of the European conference on computer vision (ECCV)*, pages 305–321, 2018. 2

[46] Hao Xu, Arbind Agrahari Baniya, Sam Well, Mohamed Reda Bouadjenek, Richard Dazeley, and Sunil Aryal. Action spotting and precise event detection in sports: Datasets, methods, and challenges. *arXiv preprint arXiv:2505.03991*, 2025. 2

[47] Hao Xu, Arbind Agrahari Baniya, Sam Wells, Mohamed Reda Bouadjenek, Richard Dazely, and Sunil Aryal. Totnet: Occlusion-aware temporal tracking for robust ball detection in sports videos. *arXiv preprint arXiv:2508.09650*, 2025. 3

[48] Jinglin Xu, Yongming Rao, Xumin Yu, Guangyi Chen, Jie Zhou, and Jiwen Lu. Finediving: A fine-grained dataset for procedure-aware action quality assessment. In *Proceedings of the IEEE/CVF conference on computer vision and pattern recognition*, pages 2949–2958, 2022. 2, 3, 5

[49] Yichao Yan, Ning Zhuang, Bingbing Ni, Jian Zhang, Ming-hao Xu, Qiang Zhang, Zheng Zhang, Shuo Cheng, Qi Tian, Yi Xu, et al. Fine-grained video captioning via graph-based multi-granularity interaction learning. *IEEE transactions on pattern analysis and machine intelligence*, 44(2):666–683, 2019. 3

[50] Fangqiu Yi, Hongyu Wen, and Tingting Jiang. Asformer: Transformer for action segmentation. In *The British Machine Vision Conference (BMVC)*, 2021. 7, 12

[51] Huanyu Yu, Shuo Cheng, Bingbing Ni, Minsi Wang, Jian Zhang, and Xiaokang Yang. Fine-grained video captioning for sports narrative. In *Proceedings of the IEEE Conference on Computer Vision and Pattern Recognition*, pages 6006–6015, 2018. 3

[52] Hongyi Zhang, Moustapha Cisse, Yann N Dauphin, and David Lopez-Paz. mixup: Beyond empirical risk minimization. *arXiv preprint arXiv:1710.09412*, 2017. 12

[53] Haotian Zhang, Cristobal Scutto, Maneesh Agrawala, and Kayvon Fatahalian. Vid2player: Controllable video sprites that behave and appear like professional tennis players. *ACM Transactions on Graphics (TOG)*, 40(3):1–16, 2021. 5

[54] He Zhu, Junwei Liang, Chengzhi Lin, Jun Zhang, and Jianming Hu. A transformer-based system for action spotting in soccer videos. In *Proceedings of the 5th international acm workshop on multimedia content analysis in sports*, pages 103–109, 2022. 1

A. Notation Table

For clarity, we provide a summary of the main symbols used throughout the paper in Table 4. This table lists the definitions of key variables (scalars, vectors, matrices, and tensors) along with evaluation parameters such as class weights and temporal tolerance, to ensure consistent interpretation of our mathematical notation.

B. Implementation Details

B.1. Backbone Model

In addition to the backbone model RegNetY-200 [25] used in all three original works—E2E-Spot [12], T-DEED [44], and UGLF [37]—we also experimented with ResNet-18 [10] as the backbone. MSAGSM is integrated into the backbone at each residual block.

B.2. Baselines

For all implementations, we adopted the publicly released code of each baseline whenever available and used the exact training configurations provided in their papers. We did observe minor performance drops compared to the results reported in the original papers, but these were marginal. Since our module is integrated directly into their official implementations without altering other components, we consider this a fair comparison.

We included ASFormer [50] as a transformer baseline, following prior work [12, 27, 44]. In earlier studies [12], ASFormer was evaluated using TSP as the feature extractor, pretrained on video action recognition datasets and then finetuned on PES. To ensure fairness, we instead used RegNetY as the feature extractor for both ASFormer and ASTRA [43], since ASTRA was originally designed to operate on pre-extracted SoccerNet features, including audio inputs.

Regarding UGLF [37], their paper utilizes additional GLIP-provided information, which is not publicly available. Therefore, we followed their released code without this input.

B.3. Training Configuration

All experiments were conducted on the same machine with a single L40S GPU. For fairness, we closely follow the training protocol of E2E-Spot [12]. Each epoch samples 5,000 clips to reduce training time while maintaining coverage of the dataset, and event frames are weighted 5 \times in the loss to address class imbalance. We train for 50 epochs using AdamW with an initial learning rate of 1×10^{-3} , a batch size of 8, and 3 warm-up epochs followed by cosine decay. As in E2E-Spot, cross-entropy loss is applied, with inputs shaped $[B, T, C, H, W]$ (batch, time, channels, height, width) and outputs $[B, T, C]$, representing frame-wise class probabilities after softmax.

B.4. Data Augmentations

During training, we randomly apply color jitter, Gaussian blur, and mixup [52]. On all datasets, frames of size 398×224 are randomly cropped to 224×224 pixels. The crop is applied only along the width dimension to preserve critical spatial information, as cropping the height could exclude important event regions. This also improves processing speed, since both the tennis court and table tennis table occupy the central region of the frame.

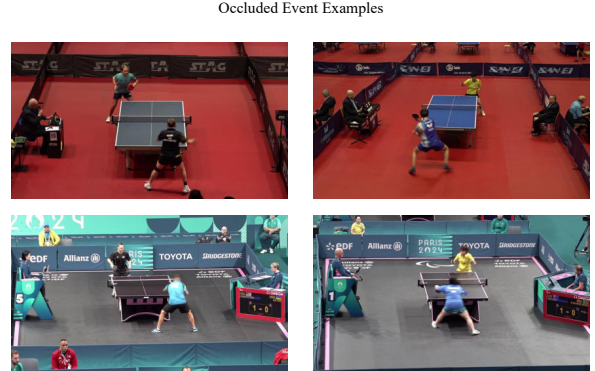


Figure 7. Examples of occluded events, when events happened during occlusion.

C. TTA Dataset

We introduce the Table Tennis Australia (TTA) dataset, the first benchmark dataset for table tennis in the PES task.

All videos in the TTA dataset were recorded and provided by the Paralympics Table Tennis Australia team. The dataset is intended strictly for research purposes and will be available upon request and approval.

It consists of 39 games, where each game is an 11-point set and each match is played as best-of-five games. We ensured diversity by including videos captured from different camera angles, with varying table and stadium colors, and across different competition levels—from elite Paralympics events to slightly lower-level WPF tournaments, which reflect broader public scenarios.

The dataset contains annotations for 8 action classes: *serve*, *forehand*, *backhand*, and *bounce*, each labeled separately for the *close table* and *far table*. Examples of each class are shown in Figure 8.

C.1. Dataset Annotation Details

Annotation was performed by three team members, with all annotations subsequently reviewed and verified by a professional sports analyst from Table Tennis Australia. For each event type, we annotated the exact frame corresponding to the critical action—for example, the frame when the

Table 4. Summary of notation used in the paper.

Symbol	Description
t	Frame index
L	Clip length (number of frames per input)
x_t	Input frame at time t
$F_t \in \mathbb{R}^{C \times H \times W}$	Feature map at frame t (C channels, $H \times W$ spatial size)
C, H, W	Number of channels, height, and width of feature maps
$X_{\text{left}}, X_{\text{right}}$	Partitioned input features for left and right shifts
$G_{\text{left}}, G_{\text{right}}$	Learned gating maps (via 3D convolution + tanh)
\odot	Element-wise (Hadamard) product
$\text{Roll}(X, \pm\delta)$	Circular shift (temporal roll) of features by δ frames left/right
δ	Temporal shift distance (in frames)
$\text{Concat}(\cdot, \cdot)$	Concatenation of feature groups along the channel dimension
\hat{X}	Updated features after gated shifts and concatenation
$\hat{X}^{(i)}$	Output from the i -th temporal scale
w_i	Learnable weight for scale i ($w_i \geq 0, \sum_i w_i = 1$)
\hat{X}_{final}	Weighted sum of multi-scale shifted features
y_t, \hat{y}_t	Ground-truth event label and predicted score at frame t
w	Class weighting factor in cross-entropy loss
δ (eval)	Temporal tolerance used in evaluation metrics

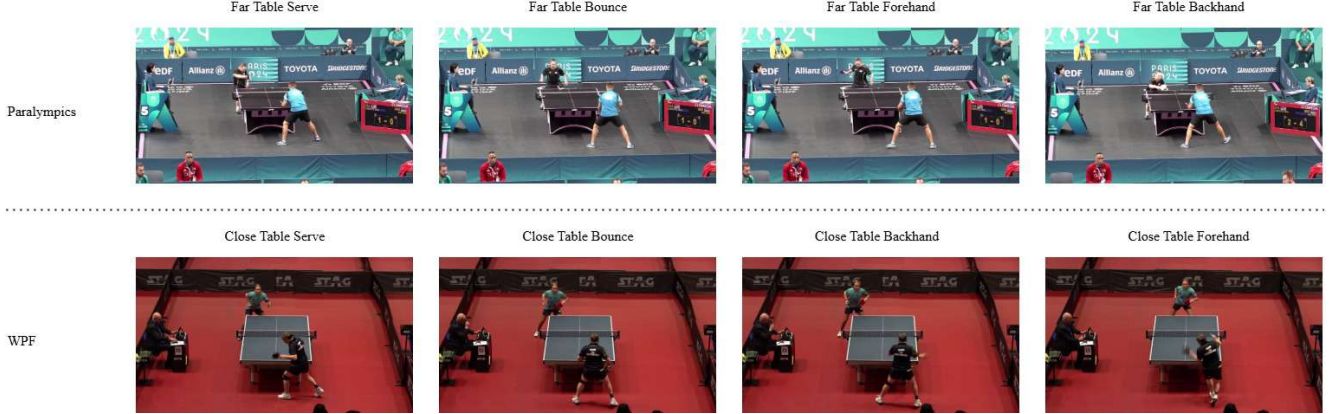


Figure 8. Examples from the TTA dataset. Each class is illustrated, with the top row showing examples from Paralympics matches and the bottom row from WPF tournaments.

ball contacts the bat for a serve, or when it lands on the table (accompanied by a sudden directional change) for a bounce.

We note that due to the frame rate of the videos, some critical moments might not be captured precisely as shown in Figure 7; in such cases, the closest possible frame was annotated. Another challenge arose from the consistent back-facing camera angle: certain events were occasionally blocked or occluded by players—such as close-table bounces or backhands. In these cases, following the proce-

dure used by professional sports analysts, we inferred the event frame based on the surrounding context in adjacent frames.

D. Additional Experiments

In this section, we provide additional experiments using ResNet-18 as the backbone within the E2E, T-DEED, and UGLF frameworks. We also report mAP@0 results across different temporal modules and datasets. Finally, we in-

Table 5. Performance comparison (mAP %) under different temporal tolerances ($\delta = 0, 1, 2$) for T-DEED and UGLF under ResNet-18 backbone. Results are reported on five fine-grained sports video datasets. The best result for each column is **bolded**, and our proposed method is *italicized*. \star indicates the best result within each model-backbone group. All models are evaluated using a fixed clip length of 100 frames.

Model	Backbone	Temp	TTA			Tennis			FS.Comp			FS.Perf			FineDiving			P (M) / GFLOPs		
			$\delta=0$	$\delta=1$	$\delta=2$	$\delta=0$	$\delta=1$	$\delta=2$												
E2E-Spot	ResNet-18	GSM	40.30	69.13	78.37	49.74	90.43	96.72	37.80	77.31	87.52	43.73	82.75	94.56	26.53	64.63	84.79	14.35 / 367.04		
E2E-Spot	ResNet-18	GSF	39.11	66.42	80.75[*]	49.32	90.48	97.01	35.50	73.21	87.37	39.04	78.50	90.58	24.31	64.25	84.01	14.35 / 367.04		
<i>E2E-Spot</i>	<i>ResNet-18</i>	<i>Ours</i>	43.81[*]	70.49[*]	79.38	52.82[*]	90.81[*]	97.52[*]	40.49 [*]	78.29[*]	90.93[*]	45.75[*]	85.23[*]	96.62[*]	30.43[*]	67.17[*]	84.95[*]	14.37 / 370.40		
T-DEED	ResNet-18	GSM	39.81 [*]	66.78	76.13	48.09	89.46 [*]	97.19	38.64 [*]	76.65 [*]	87.02	42.82 [*]	83.67 [*]	95.35	25.86	63.11	83.34	37.34 / 369.26		
T-DEED	ResNet-18	GSF	38.26	68.84	75.59	45.57	88.48	97.22	35.54	75.58	88.87 [*]	42.03	83.09	96.22	28.81 ^{**}	68.68 [*]	85.21 [*]	37.34 / 369.26		
<i>T-DEED</i>	<i>ResNet-18</i>	<i>Ours</i>	39.51	69.92[*]	77.33[*]	51.56[*]	87.18	95.85[*]	36.89	76.17	88.57	40.90	82.58	96.35[*]	23.68	66.78	84.88	37.37 / 372.62		
UGLF	ResNet-18	GSM	32.89	60.05	69.50	49.05	89.38	97.14	36.57	75.93	90.16	42.30 [*]	81.28	92.60	24.53	65.88	84.92	14.35 / 367.04		
UGLF	ResNet-18	GSF	36.98	62.58 [*]	68.57	47.59	89.11	97.31[*]	34.22	74.88	88.49	41.73	82.34 [*]	94.27	22.42	65.56	84.56	14.35 / 367.04		
UGLF	ResNet-18	<i>Ours</i>	37.14 [*]	62.30	72.14 [*]	52.14 [*]	91.06[*]	97.28	40.69[*]	77.21 [*]	90.25 [*]	40.55	81.46	94.84 [*]	29.56 [*]	68.98[*]	87.60[*]	14.37 / 370.40		

clude results for alternative dilation configurations that were not shown in the main paper.

D.1. Different Backbone

We evaluate MSAGSM with ResNet-18 as the backbone to test its effectiveness with a different feature extractor. Results in Table 5 show that MSAGSM consistently improves performance across all models, confirming its robustness to backbone choice. Out of 10 results, MSAGSM achieves 8 best scores, and across 30 groups, it achieves 20 best results—particularly excelling in the simpler E2E and UGLF models. As observed in the main results, the additional temporal information from MSAGSM may conflict with the more complex design of T-DEED, leading to less optimal gains in that setting. This suggests that T-DEED’s existing fine-grained temporal modules already capture much of the relevant temporal context, leaving little room for MSAGSM to contribute further. In some cases, the overlapping temporal mechanisms may introduce redundancy or even conflicting signals, which could hinder effective feature learning.

D.2. Exact Frame Prediction

In PES settings, mAP@0 measures whether the prediction lands exactly on the ground-truth frame. However, this is often ambiguous even for human annotators, so mAP@0 is considered a supplementary result. These results are presented in Table 5 for ResNet-18.

We observe that even under the strict mAP@0 setting, MSAGSM achieves strong results: on ResNet-18, in 10 out of 15 cases. This suggests that the module is particularly effective at pinpointing exact event moments when integrated into simpler architectures such as E2E-Spot, as it can fully leverage its multi-scale shifts and spatial attention. In contrast, in more complex models like T-DEED—which already incorporate advanced temporal mechanisms—MSAGSM may partially overlap or conflict

with existing components, slightly reducing its relative effectiveness.

D.3. Validation-Based Hyperparameter Selection

We selected our default hyperparameters by running experiments on validation sets from two datasets. As shown in Table 6, while the optimal configuration may vary across datasets due to differing characteristics, the default setting of $[1, 2, 3]$ with two attention heads provides the most consistent performance with minimal complexity overhead.

D.4. Loss Function Sensitivity Analysis

We conducted a sensitivity analysis of the Cross-Entropy (CE) loss weighting for the foreground (event) class, and also compared CE with focal loss on two datasets (Table 7). We observe that a weighting factor of 5 yields the best performance on both datasets, outperforming focal loss. This aligns with the standard practice reported in prior work such as E2E-Spot [12], T-DEED [44], and UGLF [37].

D.5. Different Temporal Window Setting

Here, we present a more detailed evaluation of temporal window settings for MSAGSM as shown in Table 8, including wider ranges such as $[1, \dots, 9]$ and skipped patterns like $[1, 2, 4, 6]$. As longer temporal distances are incorporated, the improvements become unstable and often diminish, suggesting that shifting information from nearby frames is sufficient in most cases. Notably, the configuration $[1, 2, 3]$ consistently performs best, effectively balancing short-term and moderate long-term dependencies. Smaller windows (like $[1, 2]$) fail to capture enough context, while larger windows (like $[1, \dots, 9]$) include redundant or noisy temporal information, which can confuse the model and harm precision. Thus, moderate dilation allows the model to attend to meaningful temporal cues without overfitting to irrelevant frames.

Table 6. Ablation study on attention head count and dilation range using the MSAGSM module on the TTA and FineDiving datasets in the Validation Set. All results are reported in mAP (%). We also report the average performance across the two datasets.

Setting	Value	TTA			FineDiving			Average			P (M) / GFLOPs
		mAP@0	mAP@1	mAP@2	mAP@0	mAP@1	mAP@2	Avg@0	Avg@1	Avg@2	
<i>Varying Number of Attention Heads (Dilations = [1,2,3])</i>											
Heads	1	41.97	68.08	72.26	31.72	73.03	88.28	36.85	70.56	80.27	4.50 / 44.68
Heads	2	38.78	71.67	79.37	33.72	73.58	89.77	36.25	72.63	84.57	4.51 / 45.06
Heads	3	38.48	67.23	71.59	30.68	71.29	86.32	34.58	69.26	78.96	4.51 / 45.42
Heads	4	40.13	67.20	70.87	32.98	74.81	87.81	36.56	71.01	79.34	4.52 / 45.78
Heads	8	39.91	66.61	73.54	30.26	72.67	88.20	35.09	69.64	80.87	4.55 / 47.24
<i>Varying Temporal Window Size (Heads = 2)</i>											
Distance	[1,2]	34.07	64.46	70.68	31.63	74.08	87.63	32.85	69.27	79.16	4.48 / 43.98
Distance	[1,2,3]	38.78	71.67	79.37	33.72	73.58	89.77	36.25	72.63	84.57	4.51 / 45.06
Distance	[1,...,4]	37.54	65.48	71.84	30.95	72.72	86.47	34.25	69.10	79.16	4.53 / 46.12
Distance	[1,...,5]	42.45	69.47	74.16	31.77	74.19	88.41	37.11	71.83	81.29	4.55 / 47.18
Distance	[1,...,6]	36.19	67.87	74.91	32.37	74.11	87.79	34.28	70.99	81.35	4.57 / 48.26
Distance	[1,...,9]	45.20	74.37	79.10	32.78	70.21	85.37	38.99	72.29	82.24	4.63 / 51.46

Table 7. Sensitivity analysis of the cross-entropy (CE) loss weighting factor on the TTA and FineDiving datasets. All results are reported in mAP (%).

Loss / Weight	TTA			FineDiving			
	mAP@0	mAP@1	mAP@2	mAP@0	mAP@1	mAP@2	
CE (1)	29.65	58.42	69.56	31.61	65.13	85.75	
CE (3)	32.04	60.52	73.38	27.09	67.08	83.16	
CE (5)	36.43	69.50	78.12	29.83	71.03	87.26	
CE (7)	35.50	67.83	77.15	29.76	68.97	86.63	
CE (9)	30.76	60.09	73.40	32.77	69.43	86.61	
Focal	32.54	58.65	71.72	30.71	67.93	85.94	

D.6. Class-wise Spotting Performance

The difficulty of precisely spotting events varies across event classes. In Figure 10, we present the interpolated precision-recall curves for the different classes in the TTA, Tennis, Figure Skating, and FineDiving datasets, as predicted by our default MSAGSM-E2E model.

We show both curves at a tolerance of 1 and a tolerance of 2. In the TTA dataset, the model exhibits difficulties with both-sides backhand events, while performing particularly well on bounce events. A similar pattern is observed in the Tennis dataset. This is reasonable, as bounce frames typically exhibit a distinct characteristic of sudden motion change at the ball’s location, making them easier to detect. In contrast, distinguishing between forehand and backhand is often ambiguous because some players are left-handed and others are right-handed, making the visual cues less consistent for the model.

D.7. Visualization of the Model

We visualize attention maps using Grad-CAM to highlight how each model attends to critical regions during precise

event spotting as shown in Figure 9. For table-bounce events under occlusion, baselines such as E2E, T-DEED, and UGLF often fail to focus on the relevant regions, whereas our approach consistently attends to the table area, demonstrating its ability to leverage long-range temporal context and effective attention mechanisms. Similarly, for jump-landing events, our model correctly emphasizes the skater’s feet, rather than irrelevant regions.

Table 8. Ablation study on attention head count and dilation range using the MSAGSM module on the TTA and FineDiving datasets. All results are reported in mAP (%).

Setting	Value	TTA			FineDiving			P (M) / GFLOPs
		mAP@0	mAP@1	mAP@2	mAP@0	mAP@1	mAP@2	
<i>Varying Number of Attention Heads (Dilations = [1,2,3])</i>								
Heads	1	32.90	60.99	75.38	29.91	66.36	83.47	4.50 / 44.68
Heads	2	36.43	69.50	78.12	29.83	71.03	87.26	4.51 / 45.06
Heads	3	35.98	65.87	75.87	28.68	67.93	85.11	4.51 / 45.42
Heads	4	30.34	61.01	72.98	30.19	68.72	85.16	4.52 / 45.78
Heads	8	35.26	64.19	72.94	29.03	70.06	85.91	4.55 / 47.24
<i>Varying Temporal Window Size (Heads = 2)</i>								
Distance	[1,2]	29.64	60.78	71.10	30.18	68.56	85.49	4.48 / 43.98
Distance	[1,2,3]	36.43	69.50	78.12	29.83	71.03	87.26	4.51 / 45.06
Distance	[1,3,5]	29.83	68.14	75.26	29.69	68.18	85.26	4.51 / 45.06
Distance	[1, ..., 4]	30.06	64.18	71.59	28.85	69.02	85.17	4.53 / 46.12
Distance	[1,2,4,6]	39.77	68.27	75.07	32.68	69.85	87.02	4.53 / 46.12
Distance	[1, ..., 5]	29.41	67.54	67.41	30.20	69.26	85.26	4.55 / 47.18
Distance	[1, ..., 6]	35.07	64.03	75.38	29.55	69.84	85.34	4.57 / 48.26
Distance	[1, ..., 9]	41.02	67.32	76.44	27.76	65.47	82.80	4.63 / 51.46

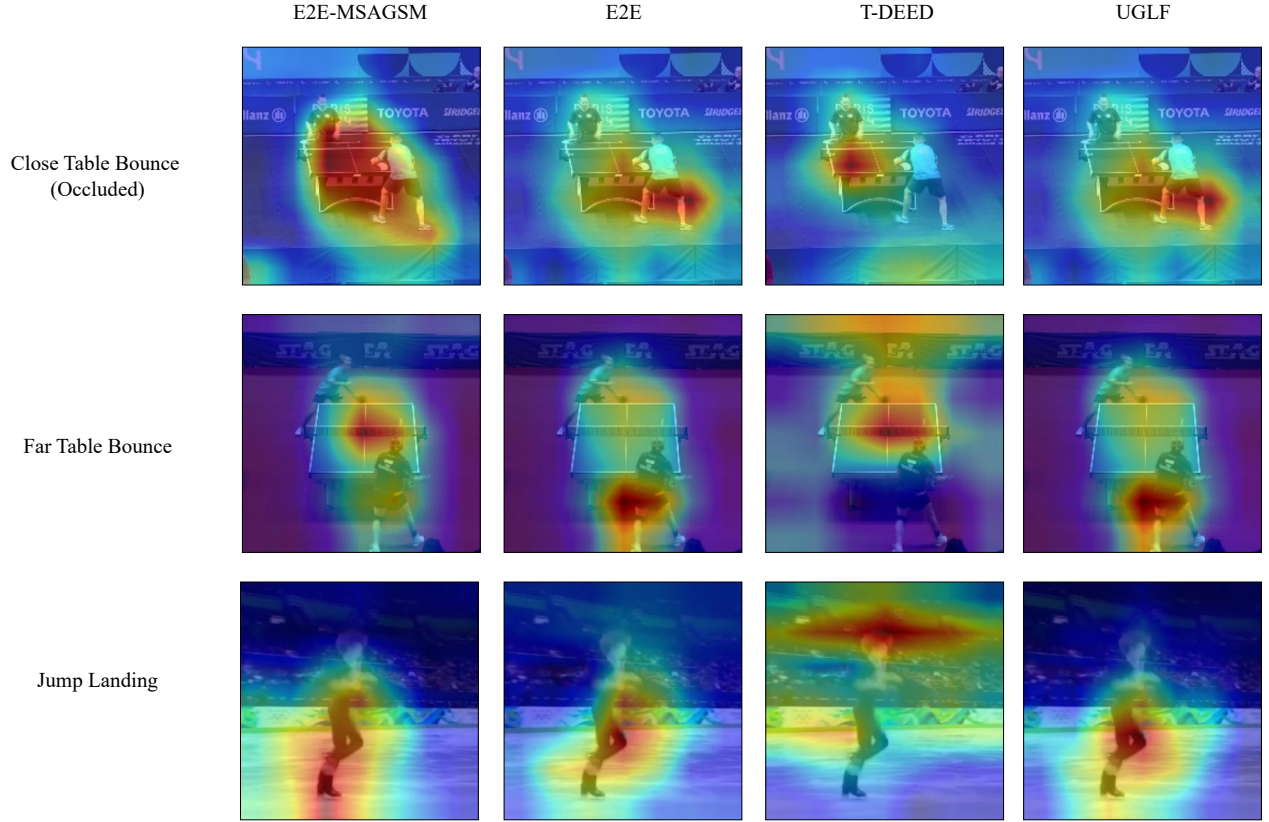
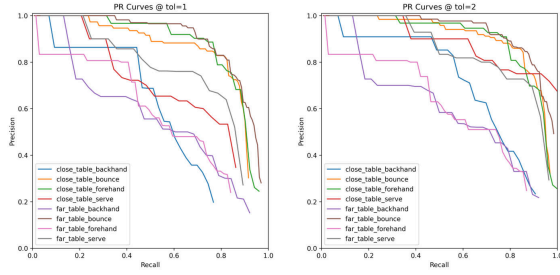
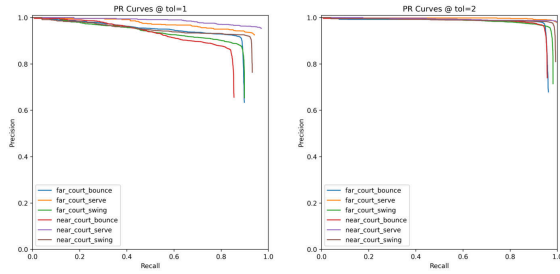


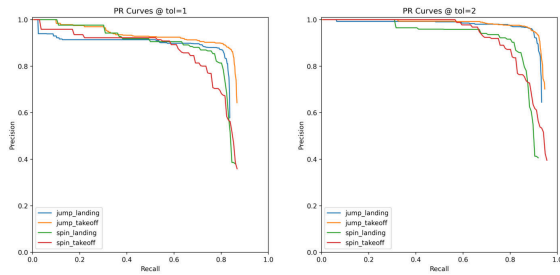
Figure 9. Grad-CAM visualizations comparing E2E-MSAGSM with baseline models (E2E, T-DEED, and UGLF) across different event types. For close table bounces under occlusion, only our model consistently attends to the correct table region, while baselines often focus elsewhere. For far table bounces, E2E-MSAGSM maintains attention on the bounce area, whereas others drift toward irrelevant regions. For jump-landing events, our model emphasizes the skater’s feet, in contrast to baselines that spread attention across less informative areas. These visualizations demonstrate the effectiveness of our module in capturing both long-range temporal context and spatially discriminative cues.



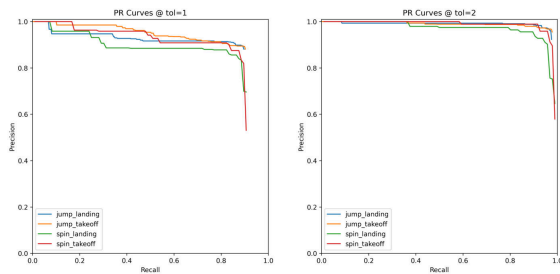
(a) TTA Curve



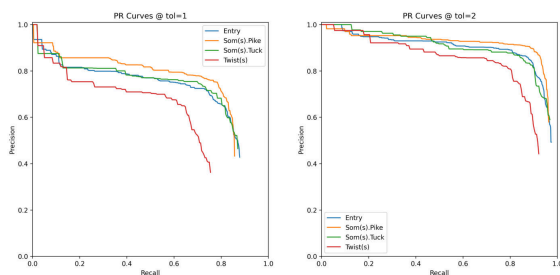
(b) Tennis Curve



(c) FS Comp Curve



(d) FS Perf Curve



(e) FineDiving Curve

Figure 10. Precision-Recall curves for different datasets. The left plot shows results at a tolerance of 1, and the right plot at a tolerance of 2.